Applied Mathematics and Computational Intelligence
Volume 14, No. 3, 2025 [79 – 95]

Three-dimensional Rotating Hybrid Nanofluid over a Shrinking Sheet with Velocity Slip

A. F. S. Raman[1], M. E. H. Hafidzuddin[1,2*], N. S. Wahid[1], N. M. Arifin[1], R. Nazar[3], I. Pop[4,5]

[1]Department of Mathematics and Statistics, Faculty of Science, Universiti Putra Malaysia, 43400 UPM Serdang, Selangor, Malaysia
[2]Centre of Foundation Studies for Agricultural Science, Universiti Putra Malaysia, 43400 UPM Serdang, Selangor, Malaysia
[3]Department of Mathematical Sciences, Faculty of Science and Technology, Universiti Kebangsaan Malaysia, 43600 Bangi, Selangor, Malaysia
[4]Department of Mathematics, Babeş-Bolyai University R-400084, Cluj-Napoca, Romania
[5]Academy of Romanian Scientists, 3 Ilfov Street 050044, Bucharest, Romania

* Corresponding author: ezadhafidz@upm.edu.my

Received: 23 August 2024
Revised: 1 September 2024
Accepted: 18 October 2024

ABSTRACT

This study deals with three dimensional rotating nanofluid over a shrinking sheet with velocity slip. Similarity transformations have been used for reducing the partial differential equations into a system of ordinary differential equations. The transformed ordinary diffential equations are solved numerically using BVP4C. The effects of Prandtl number Pr, suction parameter S, shrinking parameter λ, rotation parameter ω and slip parameter K on the velocity and temperature fields are presented and discussed in detail. The change in Prandtl number only affects the temperature profile while changing the rotation parameter affects velocity profiles. As the suction parameter rises, it results an increased velocity profile while the increase of slip parameter leads to a reduction in velocity profiles. As the Prandtl number, suction parameter, shrinking parameter, rotation parameter, and slip parameter rises, there is a reduction in the boundary layer thickness. This study provides valuable guidance and insights for researchers and practitioners investigating the mathematical or experimental aspects of three-dimensional rotating hybrid nanofluids with slip effects.

Keywords: hybrid nanofluid, rotating, shrinking sheet, slip, three-dimensional flow

1 INTRODUCTION

Nanofluids, which are colloidal suspensions of nanoparticles in a base fluid, have attracted significant attention due to their enhanced thermal and mechanical properties. The study of nanofluid flow in rotating systems has gained importance in various engineering applications such as cooling of electronic devices, lubrication systems, and heat transfer in rotating machinery. The study begins with an introduction to the basic principles of nanofluid flow, including the governing equations and boundary conditions. It discussed the role of nanoparticles in enhancing the thermal conductivity and viscosity of the base fluid, and the mechanisms governing the convective heat transfer in nanofluids. Various models, such as the single-phase approach [1] and two-phase approach [2], used

to describe nanofluid flow are presented.

Wang [3] presented a groundbreaking investigation into the three-dimensional rotating viscous flow generated by a stretching surface. Through the application of perturbation techniques, he supplied analytical solutions for fluid flow under rotation around a surface that is capable of stretching. The study then delves into the specific area of rotating nanofluid flow. It high- lights the importance of understanding the behavior of nanofluids in rotating systems and the associated challenges. Different types of rotating systems, such as rotating cylinders by Ali et al. [4], rotating disks by Ussain et al. [5], and rotating annuli by Sankar et al. [6] were discussed along with the corresponding mathematical formulations and boundary conditions. In additional, Mustafa et al. [7] discovered the effects of nonlinear thermal radiation on rotating flow of magnetite-water nanofluid, where they observed a sharp growth in heat transfer rate with increasing nonlinear thermal radiation parameter. Hayat et al. [8] investigated a rotating three-dimensional flow of hybrid nanofluid via partial slip and radiaton. They concluded that the temperature profile increases with the increase of the rotational and radiation parameter.

The theoretical study of thermal conductivity of nanofluids was introduced by Xuan and Li [9]. The volume fraction, shape, dimensions and properties of the nanoparticles affect the thermal conductivity of the nanofluid. By introducing nanoparticles, the thermal conductivity of the nanofluid can be significantly increased compared to the base fluid alone. Mathematical formulation of nanofluid was simplified by Buongiorno [10] who stated that the basic mechanics contributing to thermal enhancement are Brownian diffusion and thermophoresis. Another sub-branch of nanofluids is known to be magnetic nanofluids which have several applications in the field of engineering. This type of nanofluids were under influenced of magnetic field and gives much more interpretations of heat transfer and hydrodynamic characteristics as given by Uddin et al. [11].

The study of hybrid nanofluid, which is prepared by suspending two or more types of nanoparticles in the base fluid, was pioneered by [12–14]. Their study encompassed on alumina and copper as the hybrid nanoparticles. Hayat et al. [15] examined and compared the improvement of flow and heat transfer characteristics between a rotating nanofluid and a newly discovered hybrid nanofluid in the presence of velocity slip and thermal slip, where they observed that the velocity and temperature distributions are decreasing functions of the slip parameter, and concluded that the heat transfer rate of the hybrid nanofluid is higher as compared to the traditional nanofluid. Aly and Pop [16] concluded that when the magnetic field, suction, and copper volume fraction parameters are increased, the hybrid nanofluid leads to a greater decrease in the temperature profile compared to the mono nanofluid. Similar finding was reported by Waini et al. [17], where the skin friction and the heat transfer rate increase with the increase of copper nanoparticle.

The problem of heat and mass transfer in 3-D MHD radiative flow of water based hybrid nanofluid over an extending sheet by employing the strength of numerical computing based Lobatto IIIA method has been investigated by Shoaib et al. [18], and they found that the heat transfer rate increases with the increase in magnetic effect, Biot number and rotation parameter. Usafzai et al. [19] presented dual solutions for the two-dimension copper oxide with silver (CuO–Ag) and zinc oxide with silver (ZnO–Ag) hybrid nanofluid flow past a permeable shrinking sheet in a dusty fluid with velocity slip, where they revealed that in the scenario of decreasing flow, the wall skin friction is more pronounced in the dusty fluid as opposed to the viscous fluid. Asghar et al. [20]

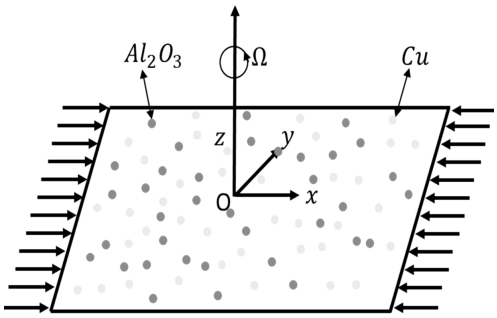

Figure 1 : Physical model

explored the influence of convective boundary conditions, viscous dissipation, thermal radiation, and heat sources/sinks on 3-D hybrid nanofluid flow across the linear stretching/shrinking sheet. They discovered that applying positive and negative increments to the rotational parameter leads to an increase in velocities for both solutions. Very recently, the problem of three-dimensional convective rotating hybrid nanofluid flow over a linear stretching/shrinking sheet under the influence of dissipative heat has been considered by Baag et al. [21]. In their research, the effects of dissipative heat that arise due to viscous dissipation and Ohmic dissipation are analyzed.

Motivated by above-mentioned studies, we intend to explore the effects of suction, rotation, shrinking, slip and Prandtl number towards a three-dimensional hybrid nanofluid with the involvements of alumina and copper nanoparticles over a shrinking sheet. The effects of the governing parameters on the primary physical quantities are presented in graphs, and thoroughly discussed in Section 3.

2 PROBLEM FORMULATION

Consider the three-dimensional rotating nanofluid past a shrinking sheet with partial slip, where x, y and z are the Cartesian coordinates, the sheet being located along the xy-plane with the z-axis measured in the vertical direction, as depicted in Fig. 1. The flow occupies the domain $z > 0$ and the sheet is shrunk in the x-directions with the velocity $u_w(x)$ and the far field (inviscid flow) velocities are $u_e(x)$ and $v_e(x)$. The sheet is rotating about z-axis with the constant angular velocity Ω and the constant mass flux velocity is w_w with $w_w < 0$ for suction and $w_w > 0$ for injection, respectively. Further, it is assumed that the surface temperature of the sheet is T_w, while the far field temperature is T_∞. The nanofluid is only partially imitating the shrinking sheet, and the fluid motion is thus subjected to the slip-flow conditions. We use here, water (H_2O as the base fluid), copper (Cu) and alumina (Al_2O_3) as thermo physical properties of the nanofluids. Under these assumptions, the following set of partial differential equations governing the continuity, momentum, and energy equations, can be expressed in the Cartesian coordinates (x, y, z) as the following [14, 22]

$$\frac{\partial u}{\partial x}+\frac{\partial v}{\partial y}+\frac{\partial w}{\partial z}=0, \tag{1}$$

$$u\frac{\partial u}{\partial x}+v\frac{\partial u}{\partial y}+w\frac{\partial u}{\partial z}-2\Omega v=\frac{\mu_{hnf}}{\rho_{hnf}}\frac{\partial^2 u}{\partial z^2}, \tag{2}$$

$$u\frac{\partial v}{\partial x}+v\frac{\partial v}{\partial y}+w\frac{\partial v}{\partial z}+2\Omega u=\frac{\mu_{hnf}}{\rho_{hnf}}\frac{\partial^2 v}{\partial z^2}, \tag{3}$$

$$u\frac{\partial T}{\partial x}+v\frac{\partial T}{\partial y}+w\frac{\partial T}{\partial z}=\frac{k_{hnf}}{(\rho C_p)_{hnf}}\frac{\partial^2 T}{\partial z^2}, \tag{4}$$

subject to the boundary conditions

$$\begin{aligned} u=u_w(x)=U(x)\lambda+u_{\text{wslip}}(x),\ v_w(x)=v_{\text{wslip}}(x),\ w=w_w,\ T=T_w \text{ at } z=0,\\ u=u_e(x)\to 0,\ v_e(x)\to 0,\ T\to T_\infty \text{ as } z\to\infty, \end{aligned} \tag{5}$$

where u, v and w are the velocity components along x, y and z axes, T is the temperature of the nanofluid, $U_w(x)=ax$, where a is a positive constant, and $\lambda<0$ is the shrinking parameter with $\lambda=0$ corresponding to the static sheet.

The velocities slips components are defined as [23]

$$u_{\text{wslip}}(x)=N\frac{\mu_{hnf}}{\rho_{hnf}}\frac{\partial u}{\partial z},\ v_{\text{wslip}}(x)=N\frac{\mu_{hnf}}{\rho_{hnf}}\frac{\partial v}{\partial z}, \tag{6}$$

where N is the slip length. Table 1 and 2 display the correlation of the physical properties [24–26] and the hybrid nanofluid's thermo-physical properties [27], respectively. Here in these tables, the hnf, f, 1 and 2 subscripts refer to the hybrid nanofluid, base fluid and solid nanoparticle for the alumina and solid nanoparticle for copper, accordingly, and ϕ_1 and ϕ_2 represent the alumina and copper volume fraction parameters, respectively.

Table 1 : Hybrid nanofluid physical properties.

Properties	**Hybrid Nanofluid Correlations**
Density	$\rho_{hnf}=\rho_1\phi_1+\rho_2\phi_2+\rho_f(1-\phi_{hnf})$, where $\phi_{hnf}=\phi_1+\phi_2$
Heat capacity	$(\rho C_p)_{hnf}=(\rho C_p)_1\phi_1+(\rho C_p)_2\phi_2+(\rho C_p)_f(1-\phi_{hnf})$
Dynamic Viscosity	$\dfrac{\mu_{hnf}}{\mu_f}=\dfrac{1}{(1-\phi_{hnf})}$
Thermal Conductivity	$\dfrac{k_hnf}{k_f}=\left[\dfrac{2k_f+\left(\frac{\phi_1k_1+\phi_2k_2}{\rho_{hnf}}\right)+2(\phi_1k_1+\phi_2k_2)-2\phi_{hnf}k_f}{2k_f-(\phi_1k_1+\phi_2k_2)+\left(\frac{\phi_1k_1+\phi_2k_2}{\rho_{hnf}}\right)+\phi_{hnf}k_f}\right]$

Guided by the boundary conditions (5), the following similarity variables are introduced

$$u=axf'(\eta),\ v=axg(\eta),\ w=-\sqrt{a\nu_f}f(\eta),\ \theta(\eta)=\frac{T-T_\infty}{T_f-T_\infty},\ \eta=z\sqrt{\frac{a}{\nu_f}}. \tag{7}$$

Table 2 : Thermo-physical properties.

Physical Properties	**Water**	**Al_2O_3**	**Cu**
ρ (kg/m^3)	997.1	3970	8933
C_p (J/kgK)	4179	765	385
k (W/mK)	0.613	40	400

Substituting (7) into Eqs. (1)-(4), Eq. (1) is satisfied, while Eqs. (2)-(4) are transformed to following ordinary (similarity) differential equations

$$\frac{\mu_{hnf}/\mu_f}{\rho_{hnf}/\rho_f} f''' + ff'' - f^2 + 2\omega g = 0, \tag{8}$$

$$\frac{\mu_{hnf}/\mu_f}{\rho_{hnf}/\rho_f} g'' + fg' - f'g - 2\omega f' = 0, \tag{9}$$

$$\frac{1}{Pr} \frac{k_{hnf}/k_f}{(\rho C_p)_{hnf}/(\rho C_p)_f} \theta'' + f\theta' = 0, \tag{10}$$

along with the boundary condition

$$\begin{aligned} &f(0) = S,\ f'(0) = \lambda + Kf''(0),\ g(0) = Kg'(0),\ \theta(0) = 1, \\ &\qquad f'(\eta) \to 0,\ g(\eta) \to 0,\ \theta(\eta) \to 0 \text{ as } \eta \to \infty. \end{aligned} \tag{11}$$

Here $Pr = \frac{(\rho C_p)_f}{k_f}$ is the Prandtl number, $\omega = \Omega/a$ is the angular velocity of the hybrid nanofluid and $K = N\sqrt{a\nu_f}$ is the slip parameter.

It is worth mentioning that for $\phi_1 = \phi_2 = 0$ (classical viscous fluid) and if $K = 0$, there is no slip i.e., velocity of the fluid and the sheet is the same and then boundary conditions (11) are reduced to those of [3] and [28]. If $K \to \infty$, the surface is stress-free indicating no flow at all.

The quantities of physical interest are the skin friction coefficient C_{fx} along the x-axis, C_{fy} along the y-axis and the local Nusselt number, which are defined as

$$\begin{aligned} C_{fx} = \frac{\mu_{hnf}}{\rho_f u_w^2(x)} \left(\frac{\partial u}{\partial z}\right)_{z=0},\ C_{fy} = \frac{\mu_{hnf}}{\rho_f u_w^2(x)} \left(\frac{\partial \nu}{\partial z}\right)_{z=0}, \\ Nu_x = \frac{x k_{hnf}}{k_f(T_w - T_\infty)} \left(-\frac{\partial T}{\partial z}\right)_{z=0}. \end{aligned} \tag{12}$$

Using (7), we get

$$Re_x^{1/2} C_{fx} = \frac{\mu_{hnf}}{\mu_f} f''(0),\ Re_x^{1/2} C_{fy} = \frac{\mu_{hnf}}{\mu_f} g''(0),\ Re_x^{-1/2} Nu_x = -\frac{k_{hnf}}{k_f} \theta'(0), \tag{13}$$

where $Re_x = u_w(x)/\nu_f$ is the local Reynolds number.

3 RESULTS AND DISCUSSION

The bvp4c solver in MATLAB is employed to assess the numerical solutions for Eqs. (8)-(10) under the specified boundary conditions (11). In order to compute the most accurate results, it is necessary to carefully select and fine-tune appropriate initial guesses, preferred boundary layer thickness, and various parameter values within the coding function of the solver. Throughout this study, the shrinking parameter, Prandtl number, and nanoparticle volume fraction for alumina remain constant, set at $\lambda = -1$, $Pr = 6.2$, and $\phi_1 = 0.01$, respectively. Conversely, parameters like the nanoparticle volume fraction for copper ϕ_2, suction S, rotation parameter ω, and slip parameter K are varied to analyze their effects on boundary layer flow and heat transfer.

To validate our findings, we compare the numerical values of $Re_x^{1/2}C_{fx}$ and $Re_x^{-1/2}Nu_x$ from this study with previous results reported by Devi and Devi [12, 14], as depicted in Table 3. Specifically, we examine the case of Cu-water ($\phi_1 = 0, \phi_2 = 0.04$) on a stretching surface ($\lambda = 1$), with $\omega = K = 0$ and $Pr = 6.135$. Another comparison was made for the case of viscous fluid ($\phi_1 = \phi_2 = 0$) and stretching sheet ($\lambda = 1$) with Asghar et al. [20] by setting $Pr = 6.2$, $S = 0$ and $K = 0$, as shown in Table 4. We find a satisfactory correlation between the present findings and those of previous studies. Thus, we can confidently assert the validity and acceptability of the technique and results presented in this study.

Table 3 : Comparison of skin friction coefficient and local Nusselt number for Cu-Water ($\phi_1 = 0, \phi_2 = 0.04$) when $\lambda = 1$, $\omega = K = 0$ and $Pr = 6.135$.

	[12]		[14]		Present results	
S	$Re_x^{1/2}C_{fx}$	$Re_x^{-1/2}Nu_x$	$Re_x^{1/2}C_{fx}$	$Re_x^{-1/2}Nu_x$	$Re_x^{1/2}C_{fx}$	$Re_x^{-1/2}Nu_x$
0.5	−1.582096	4.132241	–	–	−1.582070230	4.132244667
0	–	–	−1.208432	1.822984	−1.208325024	1.823025913

Table 4 : Comparison of the present values of $f''(0)$ and $g'(0)$ with Asghar et al. [20] when $\phi_1 = \phi_2 = 0$, $\lambda = 1$, $K = 0$ and $Pr = 6.2$.

	[20]		Present findings	
ω	$f''(0)$	$g'(0)$	$f''(0)$	$g'(0)$
0	−1	0	−1	0
0.5	−1.13837	−0.512760	−1.138374180	−0.512760732
1.0	−1.325028	−0.837098	−1.325028720	−0.837098263
1.5	−1.496403	−1.082978	−1.496403757	−1.082978655
2.0	−1.652352	−1.287258	−1.652351998	−1.287258831
2.5	−1.795728	−1.465217	−1.795728182	−1.465217196
3.0	−1.928931	−1.624735	−1.928931455	−1.624735752

Figs. 3-5 display the velocity profiles $f'(\eta)$ and $g(\eta)$ and temperature profiles $\theta(\eta)$, respectively, for different values of rotation parameter ω when $\phi_1 = \phi_2 = 0.01$, $S = 3$, $\lambda = -1$, $K = 0.2$ and $Pr = 6.135$. The increase in ω leads to decrease in boundary layer thickness, as illustrated in the Figs. 3 and 5, while the opposite effect is observed in Fig. 4. This occurs because rotation introduces additional forces, including centrifugal and Coriolis forces, which can impact the boundary layer thickness. These forces have the potential to affect the fluid near the surface, either reducing or

increasing the thickness of the boundary layer.

The effects of slip parameter K is demonstrated throughout Figs. 6-8 when $\phi_1 = \phi_2 = 0.01$, $S = 3$, $\lambda = -1$, $\omega = 0.2$ and $Pr = 6.135$. Like the previous figures, it seems that the increase of slip parameter causes the reduction in boundary layer thickness in $f'(\eta)$ and $\theta(\eta)$, but not $g(\eta)$. This happens because slip enables fluid particles to move more effortlessly across the surface, decreasing flow resistance and leading to a thinner boundary layer. However for the lateral velocity $g(\eta)$, fluid particles near the surface experience reduced friction, allowing them to slide more easily. This increased mobility can lead to the formation of vortices or disturbances in the flow, causing mixing and entrainment of outer fluid into the boundary layer. As a result, the boundary layer thickness is increasing due to the additional fluid being drawn into it.

Moreover, the influence of suction parameter S against the velocity and temperature profiles when $\phi_1 = \phi_2 = 0.01$, $K = 0.6$, $\lambda = -1$, $\omega = 0.2$ and $Pr = 6.135$ is demonstrated in Figs. 9-11. It is found in these figures that the increment in suction parameter causes the thinning of boundary layer thickness. This happens because suction is pulling away some of the slow-moving air near the surface, which then creates space for faster-moving air from further away to replace it, resulting in a thinner boundary layer.

In addition, the increase of the copper volume fraction parameter $\phi_2 (= 0.01, 0.015, 0.02)$ causes the decrement in boundary and thermal layer thickness, as displayed in Figs. 12-14. Typically, as the copper volume fraction rises, the fluid's viscosity decreases. This reduction in viscosity translates to reduced flow resistance, leading to increased velocities throughout the flow field. Additionally, copper nanoparticles exhibit higher thermal conductivity in comparison to the base fluid. Therefore, with an increase in the volume fraction of copper, the fluid's thermal conductivity also rises. As a result, heat is more effectively transferred within the fluid, resulting in an enhancement of the temperature profiles.

Finally, the effects of Prandtl number Pr against $f''(0)$, $g'(0)$ and $-\theta'(0)$ as well as the temperature profile $\theta(\eta)$ are depicted in Table 5 and Fig. 2, respectively. The rise in Pr evidently results in a higher local Nusselt number, as displayed in Table 5. Higher Prandtl numbers improve the convective heat transfer coefficient due to the more effective momentum transfer relative to heat diffusion, which enhances the overall heat transfer rate. Moreover, Fig. 2 shows that the increase of Pr leads to the thinner thermal boundary layer, resulting in a steeper temperature gradient at the surface. A steeper temperature gradient at the surface enhances the rate of heat transfer from the surface to the fluid, which increases the local Nusselt number, which supports the previous statement.

4 CONCLUSION

The three-dimensional rotating nanofluid over a shrinking sheet with velocity slip has been considered and solved numerically using a BVP4C function in Matlab. The followings are the findings that can be summarized from this study:

1. As the suction parameter rises, it results an increased velocity profile $f'(\eta)$, a decreased

Table 5 : The values of $f''(0)$, $g'(0)$ and $-\theta'(0)$ for Pr when $\phi_1 = 0.01$, $\phi_2 = 0.2$, $S = 3$, $\lambda = -1$, $\omega = 0.2$ and $K = 0.2$

Pr	$f''(0)$	$g'(0)$	$-\theta'(0)$
1	2.071592016	0.049697313	1.560387507
3	2.071592016	0.049697313	4.752130960
5	2.071592016	0.049697313	7.973845095
6.2	2.071592016	0.049697313	9.912304453
8	2.071592016	0.049697313	12.823841998
10	2.071592016	0.049697313	16.062044175

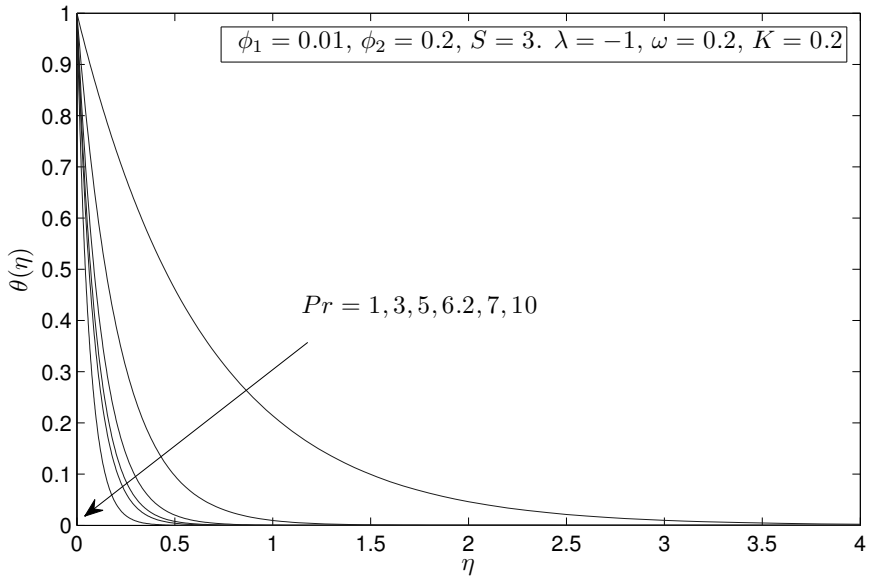

Figure 2 : Temperature profiles $\theta(\eta)$ for varied Pr

velocity profile $g(\eta)$, while slip parameter leads to a reduction in both of velocity profiles. Both of parameter results an increase in the temperature profile $\theta(\eta)$.

2. The increase of suction parameter, shrinking parameter, rotation parameter and slip parameter results in a reduction of the boundary layer thickness.

3. The increase of copper volume fraction parameter reduces the boundary layer thickness but widen the thermal boundary layer thickness.

4. The increase in the Prandtl number leads to a thinner thermal boundary layer and a steeper temperature gradient at the surface.

ACKNOWLEDGEMENT

We would like to thank Reviewers for taking the necessary time and effort to review the manuscript. We sincerely appreciate all your valuable comments and suggestions, which helped us in improving the quality of the manuscript.

REFERENCES

[1] J. Buongiorno, "Convective Transport in Nanofluids," *Journal of Heat Transfer*, vol. 128, no. 3, pp. 240–250, 08 2005. [Online]. Available: https://doi.org/10.1115/1.2150834

[2] R. K. Tiwari and M. K. Das, "Heat transfer augmentation in a two-sided lid-driven differentially heated square cavity utilizing nanofluids," *International Journal of Heat and Mass Transfer*, vol. 50, no. 9, pp. 2002–2018, 2007. [Online]. Available: https://www.sciencedirect.com/science/article/pii/S001793100600576X

[3] C. Wang, "Stretching a surface in a rotating fluid," *Z. angew. Math. Phys.*, vol. 39, p. 177–185, 1988.

[4] A. Ali, N. Amin, and I. Pop, "The unsteady boundary layer flow past a circular cylinder in micropolar fluids," *International Journal of Numerical Methods for Heat & Fluid Flow*, vol. 17, no. 7, pp. 692–714, 2007. [Online]. Available: https://doi.org/10.1108/09615530710777967

[5] S. Hussain, M. Kamal, and F. Ahmad, "The accelerated rotating disk in a micropolar fluid flow," *Applied Mathematics*, vol. 5, no. 1, pp. 196–202, 2014. [Online]. Available: http://dx.doi.org/10.4236/am.2014.51020

[6] M. Sankar, H. Kumara Swamy, Q. Al-Mdallal, and A. Wakif, "Non-darcy nanoliquid buoyant flow and entropy generation analysis in an inclined porous annulus: Effect of source-sink arrangement," *Alexandria Engineering Journal*, vol. 68, pp. 239–261, 2023. [Online]. Available: https://www.sciencedirect.com/science/article/pii/S1110016823000303

[7] M. Mustafa, A. Mushtaq, T. Hayat, and A. Alsaedi, "Rotating flow of magnetite-water nanofluid over a stretching surface inspired by non-linear thermal radiation," *PLOS ONE*, vol. 11, no. 2, pp. 1–16, 02 2016. [Online]. Available: https://doi.org/10.1371/journal.pone.0149304

[8] T. Hayat, T. Muhammad, S. A. Shehzad, and A. Alsaedi, "On magnetohydrodynamic flow of nanofluid due to a rotating disk with slip effect: A numerical study," *Computer Methods in Applied Mechanics and Engineering*, vol. 315, pp. 467–477, 2017. [Online]. Available: https://www.sciencedirect.com/science/article/pii/S0045782516312208

[9] Y. Xuan and Q. Li, "Heat transfer enhancement of nanofluids," *International Journal of Heat and Fluid Flow*, vol. 21, no. 1, pp. 58–64, 2000. [Online]. Available: https://www.sciencedirect.com/science/article/pii/S0142727X99000673

[10] N. A. Alreshidi, Z. Shah, A. Dawar, P. Kumam, M. Shutaywi, and W. Watthayu, "Brownian motion and thermophoresis effects on mhd three dimensional nanofluid flow with slip

conditions and joule dissipation due to porous rotating disk," *Molecules*, vol. 25, no. 3, 2020. [Online]. Available: https://www.mdpi.com/1420-3049/25/3/729

[11] M. J. Uddin, O. A. Bég, A. Aziz, and A. I. M. Ismail, "Group analysis of free convection flow of a magnetic nanofluid with chemical reaction," *Mathematical Problems in Engineering*, vol. 2015, p. 621503, 2015. [Online]. Available: https://doi.org/10.1155/2015/621503

[12] S. P. A. Devi and S. S. U. Devi, "Numerical investigation of hydromagnetic hybrid cu – al2o3/water nanofluid flow over a permeable stretching sheet with suction," *International Journal of Nonlinear Sciences and Numerical Simulation*, vol. 17, no. 5, pp. 249–257, 2016. [Online]. Available: https://doi.org/10.1515/ijnsns-2016-0037

[13] S. S. U. Devi and S. A. Devi, "Numerical investigation of three-dimensional hybrid cu–al2o3/water nanofluid flow over a stretching sheet with effecting lorentz force subject to newtonian heating," *Canadian Journal of Physics*, vol. 94, no. 5, pp. 490–496, 2016. [Online]. Available: https://doi.org/10.1139/cjp-2015-0799

[14] S. P. A. Devi and S. S. U. Devi, "Heat transfer enhancement of cu al2o3/water hybrid nanofluid flow over a stretching sheet," *Journal of the Nigerian Mathematical Society*, vol. 36, no. 2, pp. 419–433, 2017.

[15] T. Hayat, S. Nadeem, and A. U. Khan, "Rotating flow of ag-cuo/h2o hybrid nanofluid with radiation and partial slip boundary effects," *The European Physical Journal E*, vol. 41, no. 6, p. 75, 2018. [Online]. Available: https://doi.org/10.1140/epje/i2018-11682-y

[16] E. H. Aly and I. Pop, "Mhd flow and heat transfer over a permeable stretching/shrinking sheet in a hybrid nanofluid with a convective boundary condition," *International Journal of Numerical Methods for Heat & Fluid Flow*, vol. 29, no. 9, pp. 3012–3038, Jan. 2019. [Online]. Available: https://doi.org/10.1108/HFF-12-2018-0794

[17] I. Waini, A. Ishak, and I. Pop, "Hybrid nanofluid flow induced by an exponentially shrinking sheet," *Chinese Journal of Physics*, vol. 68, pp. 468–482, 2020. [Online]. Available: https://www.sciencedirect.com/science/article/pii/S0577907319310160

[18] M. Shoaib, M. A. Z. Raja, M. T. Sabir, S. Islam, Z. Shah, P. Kumam, and H. Alrabaiah, "Numerical investigation for rotating flow of mhd hybrid nanofluid with thermal radiation over a stretching sheet," *Scientific Reports*, vol. 10, no. 1, p. 18533, 2020. [Online]. Available: https://doi.org/10.1038/s41598-020-75254-8

[19] W. K. Usafzai, I. Pop, and C. Revnic, "Dual solutions for the two-dimension copper oxide with silver (cuo-g) and zinc oxide with silver (no-g) hybrid nanofluid flow past a permeable shrinking sheet in a dusty fluid with velocity slip," *International Journal of Numerical Methods for Heat & Fluid Flow*, vol. 34, no. 1, pp. 259–279, Jan. 2024. [Online]. Available: https://doi.org/10.1108/HFF-08-2023-0473

[20] A. Asghar, N. Vrinceanu, T. Yuan Ying, L. Ali Lund, Z. Shah, and V. Tirth, "Dual solutions of convective rotating flow of three-dimensional hybrid nanofluid across the linear

stretching/shrinking sheet," *Alexandria Engineering Journal*, vol. 75, pp. 297–312, 2023. [Online]. Available: https://www.sciencedirect.com/science/article/pii/S1110016823004568

[21] S. Baag, S. R. Mishra, P. K. Pattnaik, and S. Panda, "Three-dimensional convective rotating hybrid nanofluid flow across the linear stretching/shrinking sheet due to the impact of dissipative heat," *Pramana*, vol. 98, no. 1, p. 21, 2024. [Online]. Available: https://doi.org/10.1007/s12043-023-02717-8

[22] S. Nadeem, A. U. Rehman, R. Mehmood, and M. A. Sadiq, "Partial slip effects on a rotating flow of two phase nano fluid over a stretching surface," *Current Nanoscience*, vol. 10, no. 6, pp. 846–854, 2014.

[23] S. Mukhopadhyay and H. I. Andersson, "Effects of slip and heat transfer analysis of flow over an unsteady stretching surface," *Heat and Mass Transfer*, vol. 45, no. 11, pp. 1447–1452, 2009. [Online]. Available: https://doi.org/10.1007/s00231-009-0516-7

[24] B. Takabi and S. Salehi, "Augmentation of the heat transfer performance of a sinusoidal corrugated enclosure by employing hybrid nanofluid," *Advances in Mechanical Engineering*, vol. 6, p. 147059, 2014. [Online]. Available: https://doi.org/10.1155/2014/147059

[25] T. Tayebi and A. Chamkha, "Entropy generation analysis during mhd natural convection flow of hybrid nanofluid in a square cavity containing a corrugated conducting block," *International Journal of Numerical Methods for Heat & Fluid Flow*, vol. 30, no. 3, pp. 1115–1136, 2020.

[26] M. Ghalambaz, N. C. Rosca, A. V. Rosca, and I. Pop, "Mixed convection and stability analysis of stagnation-point boundary layer flow and heat transfer of hybrid nanofluids over a vertical plate," *International Journal of Numerical Methods for Heat & Fluid Flow*, vol. 30, no. 7, pp. 3737–3754, 2020. [Online]. Available: https://doi.org/10.1108/HFF-08-2019-0661

[27] H. F. Oztop and E. Abu-Nada, "Numerical study of natural convection in partially heated rectangular enclosures filled with nanofluids," *International Journal of Heat and Fluid Flow*, vol. 29, no. 5, pp. 1326–1336, 2008. [Online]. Available: https://www.sciencedirect.com/science/article/pii/S0142727X08000933

[28] R. Sharma, A. Ishak, and I. Pop, "Partial slip flow and heat transfer over a stretching sheet in a nanofluid," *Mathematical Problems in Engineering*, vol. 2013, p. 724547, 2013.

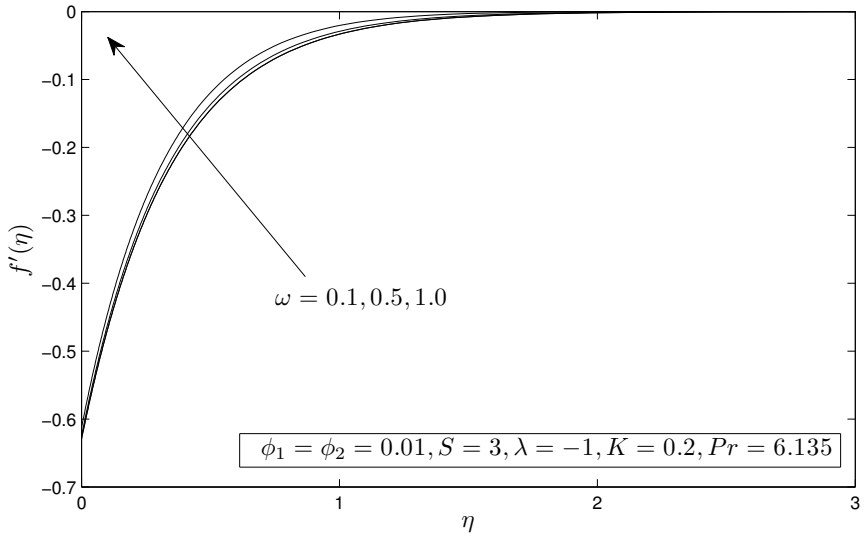

Figure 3 : Velocity profiles $f'(\eta)$ for varied ω

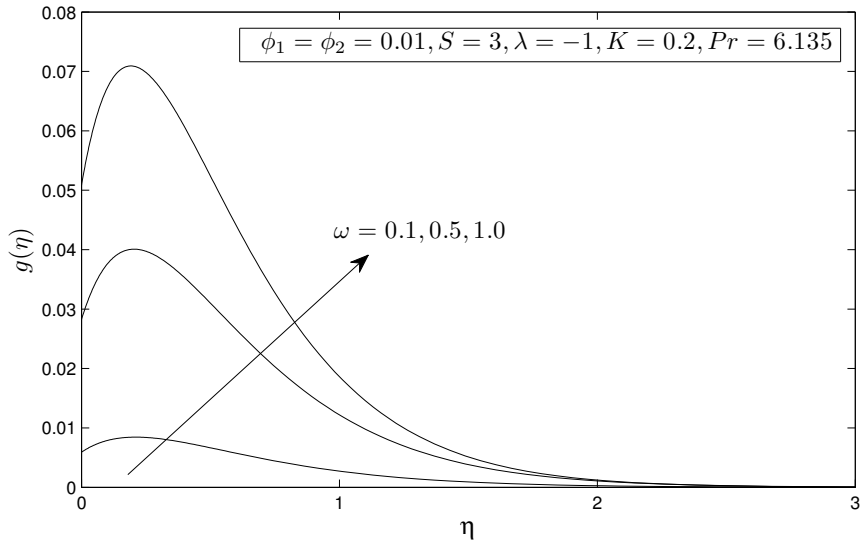

Figure 4 : Velocity profiles $g(\eta)$ for varied ω

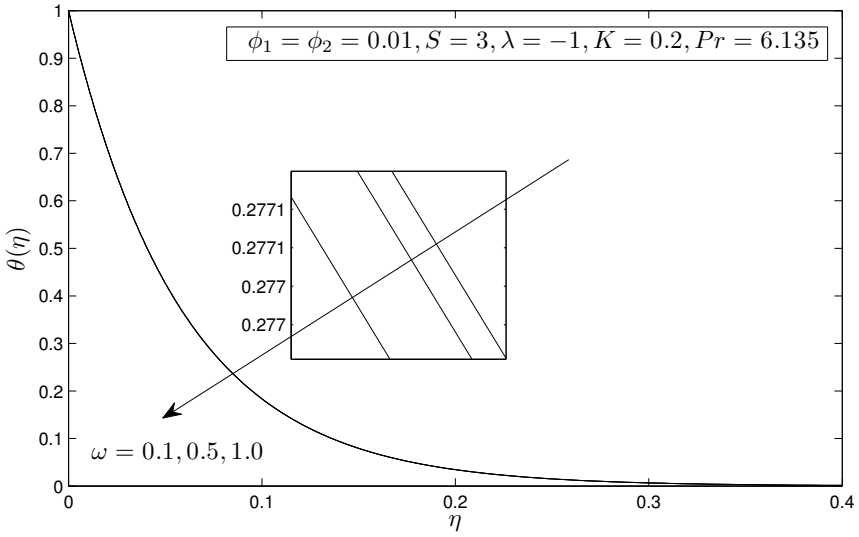

Figure 5 : Temperature profiles $\theta(\eta)$ for varied ω

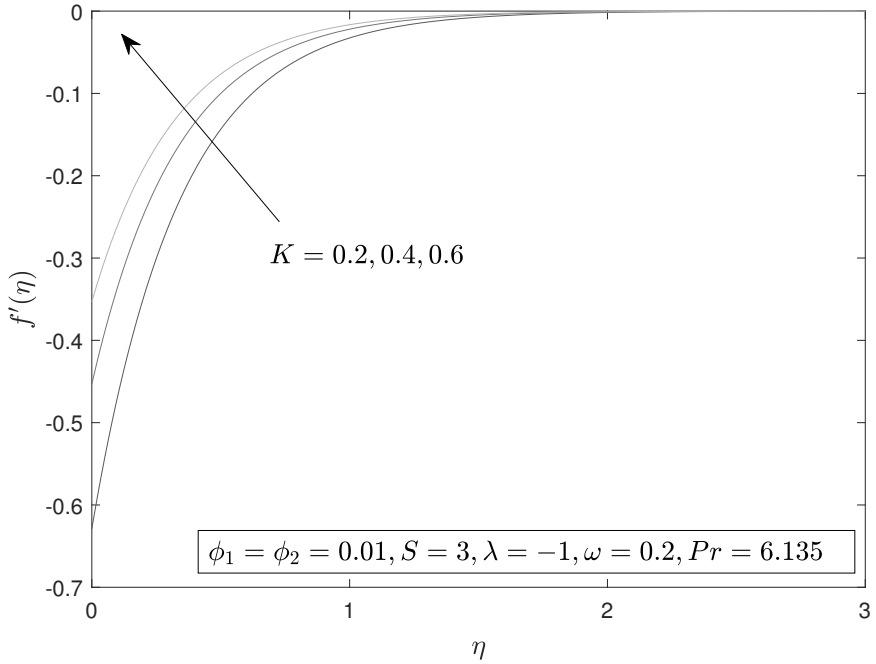

Figure 6 : Velocity profiles $f'(\eta)$ for varied K

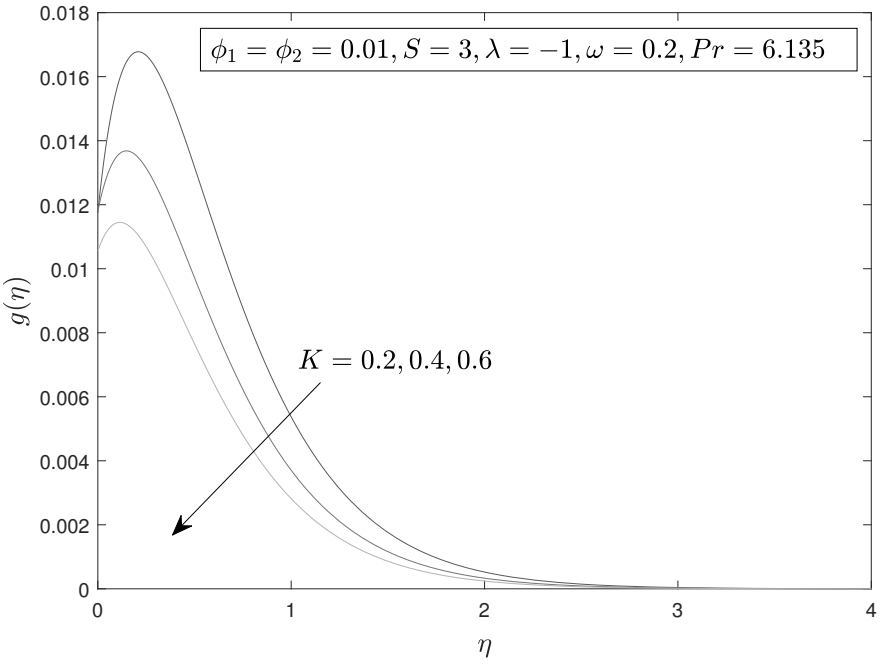

Figure 7 : Velocity profiles $g(\eta)$ for varied K

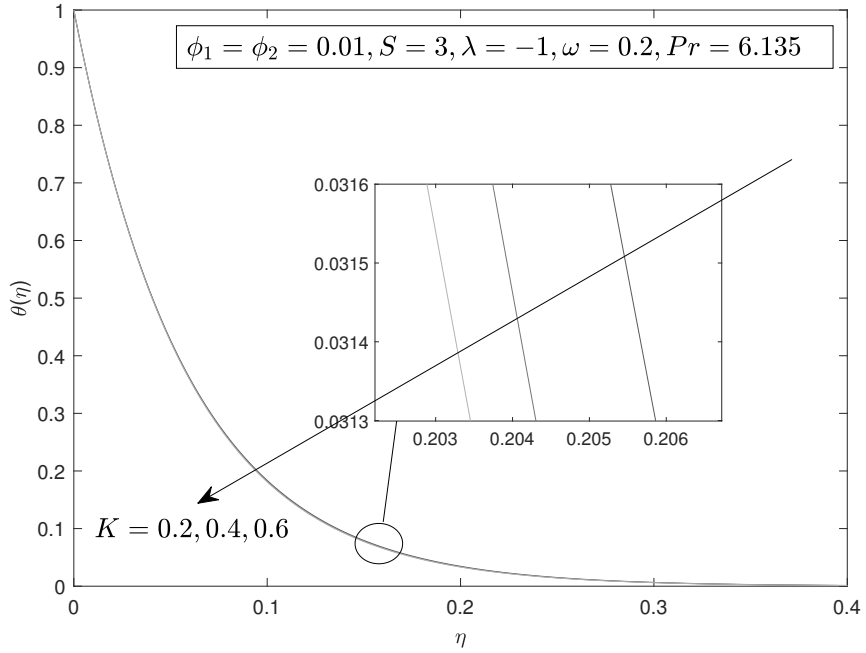

Figure 8 : Temperature profiles $\theta(\eta)$ for varied K

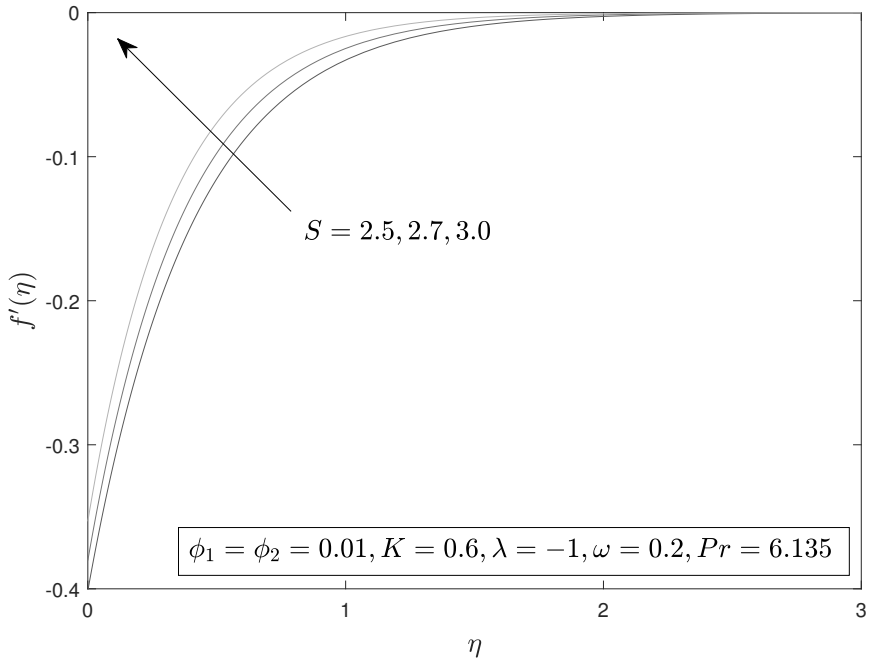

Figure 9 : Velocity profiles $f'(\eta)$ for varied S

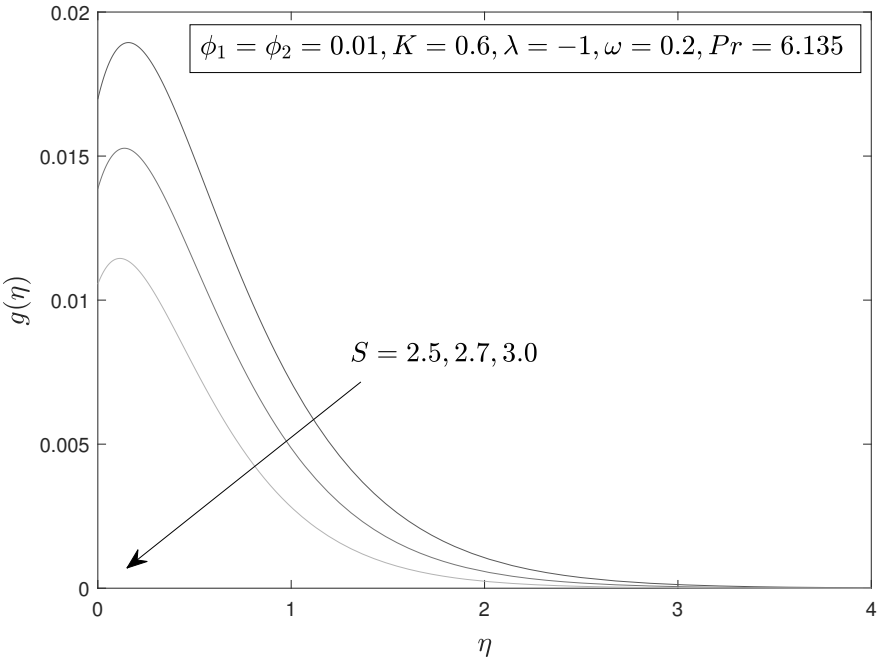

Figure 10 : Velocity profiles $g(\eta)$ for varied S

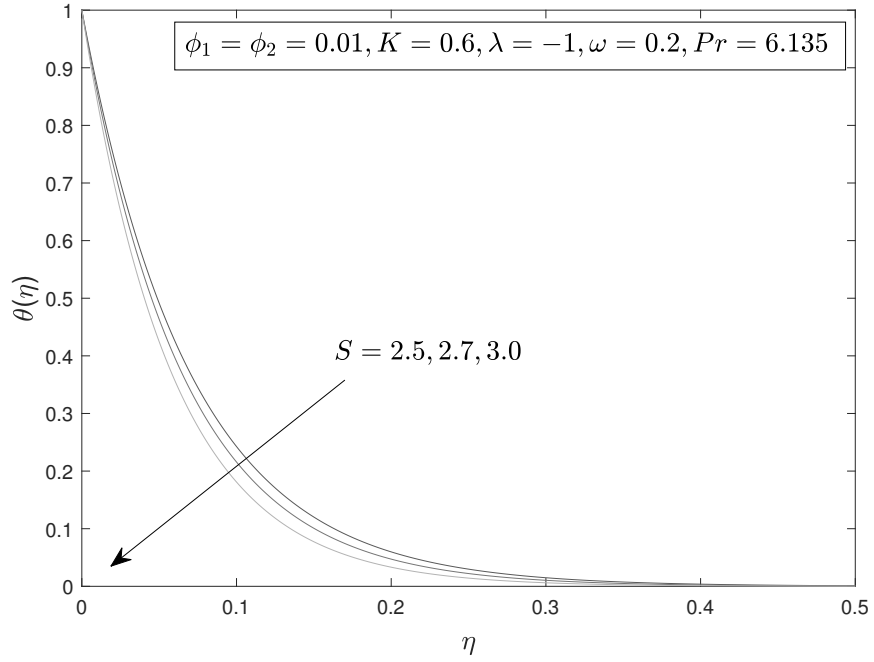

Figure 11 : Temperature profiles $\theta(\eta)$ for varied S

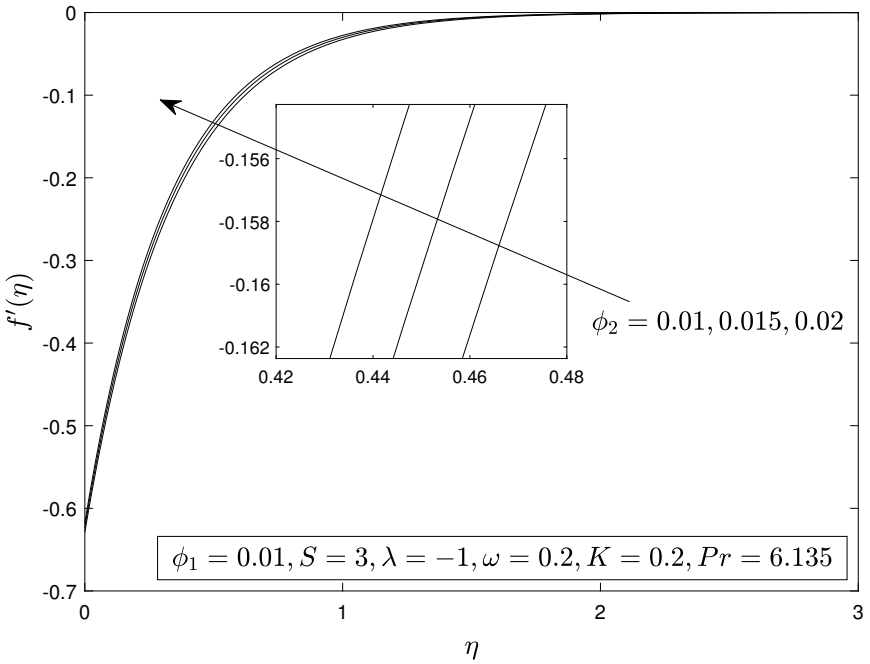

Figure 12 : Velocity profiles $f'(\eta)$ for varied ϕ_2

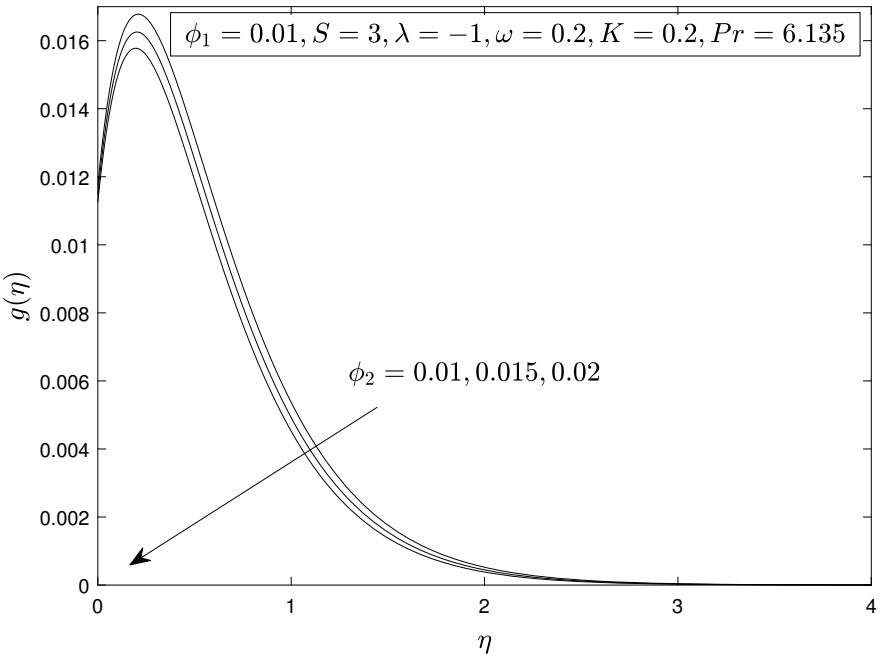

Figure 13 : Velocity profiles $g(\eta)$ for varied ϕ_2

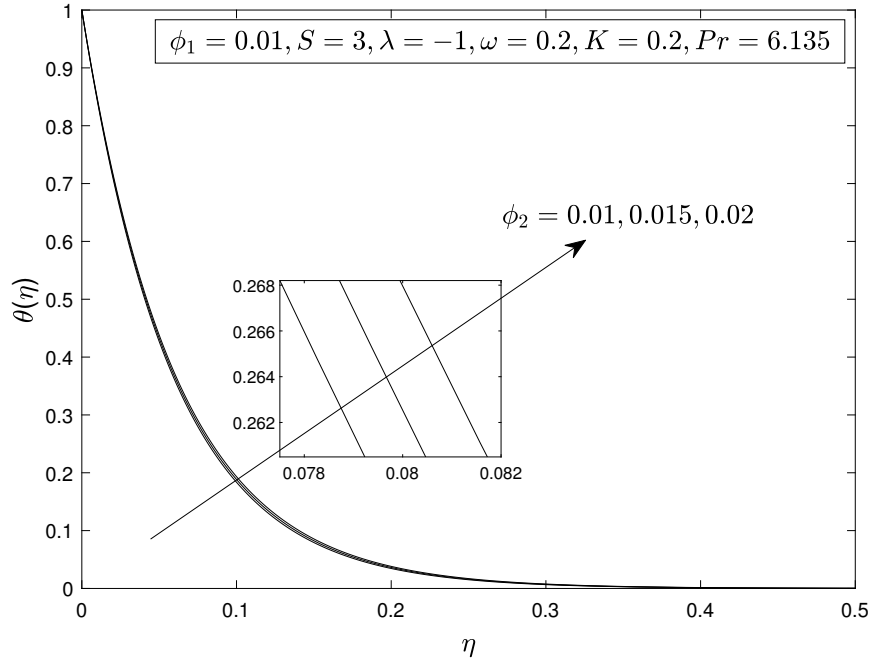

Figure 14 : Temperature profiles $\theta(\eta)$ for varied ϕ_2